Composites: Part A 173 (2023) 107679

Contents lists available at ScienceDirect

Composites Part A

journal homepage: www.elsevier.com/locate/compositesa

Tailored flexibility in inherently brittle epoxy-based composites through gradient interphase formation with bio-based thermoplastic elastomer grades

Lucian Zweifel *, Julian Kupski, Christian Brauner

Institute of Polymer Engineering, FHNW University of Applied Sciences and Arts Northwestern Switzerland, Windisch, Switzerland

ARTICLE INFO

Keywords:
Multifunctional composites (A)
Interface/interphase (B)
Microstructures (B)
Microstructural analysis (D)
3-D Printing (E)
Vacuum Infusion (E)

ABSTRACT

This study focuses on tailoring elastic behaviour in an inherently brittle epoxy-based fibre-reinforced composite material formed through a gradient interphase with a bio-based thermoplastic elastomer. The fast-curing epoxy Araldite LY3585/Aradur 3475 was tested with two bio-based Pebax block copolymer grades. First, the interphase was characterised via optical hot-stage microscopy and Raman spectroscopy. The analysis unveiled pronounced diffusion followed by a reaction-induced phase separation, which led to the formation of an interphase with a thickness exceeding 200 μm at the temperatures associated with the curing process. Second, composite laminates were fabricated through a combined process of fused filament fabrication and vacuum infusion, incorporating a flexible domain with variable stiffness properties. The material architecture exhibited brittle-to-ductile behaviour at the micrometre scale, with tailored flexible response under bending and stiff behaviour in tension. Consequently, the study anticipates using multi-scale toughened material structures for more efficient generative design concepts.

1. Introduction

Fibre-reinforced composites are important structural materials for future sustainable transportation, energy storage, construction, and biomedical technologies owing to their excellent combination of significantly reduced weight and improved mechanical performance. However, a considerable challenge arises because synthetic materials cannot be simultaneously strong and tough, as both properties do not co-exist [1]. Consequently, highly cross-linked thermoset composites tend to be brittle or notch-sensitive, with a low resistance to crack initiation and growth [1,2]. Therefore, different strategies have been developed to improve the fracture toughness of brittle epoxy systems [1–6]: (a) varying the cross-link density and initial molecular chain lengths of the epoxy resin, (b) incorporation of a rubbery phase (i.e. elastomer), (c) inclusion of a thermoplastic phase, (d) and inclusion of nanofillers such as graphene nanoplatelets and hyperbranched polymer nanoparticles. A second polymer (ductile phase) incorporated in the epoxy matrix can act as a toughening agent to prevent crack propagation, thus improving the fracture toughness. Despite this, the addition of materials such as liquid rubbers results in the loss of thermal stability owing to the lower glass transition temperature (Tg) of the added phase. Therefore, toughening agents such as amorphous thermoplastics (e.g. polyetherimide (PEI) and polyethersulfone (PES)) have been investigated intensively [2,4,5,7,8]. At the start of the reaction, the uncured epoxy and soluble thermoplastic polymer undergo mutual diffusion, with the epoxy diffusing into the thermoplastic and causing swelling [9,10]. As curing progresses, the molecular weight of the epoxy increases, reducing their ability to diffuse. The curing temperature triggers a reaction-induced phase separation, which occurs when the composition line crosses the curing temperature. The phase separation process is influenced by thermodynamics, kinetics, and the time-dependent viscosity of the thermoset matrix, leading to the formation of microregions with slight compositional deviations from the system composition [9,11]. Existing literature suggests two primary mechanisms for phase separation: nucleation and growth, and spinodal decomposition. The onset of phase separation is temperature-dependent, with higher temperatures delaying the initiation of phase separation due to increased chain mobility. The interphase thickness increases with temperature until it reaches a maximum due to the reactivity of the epoxy. The phase separation does not coincide along the diffusion length due to the concentration profile, resulting in a graded interphase morphology. The final morphology is determined by the competition between the increase in epoxy molecular weight, which

* Corresponding author at: Klosterzelgstrasse 2, 5210 Windisch, Switzerland.
E-mail address: lucian.zweifel@fhnw.ch (L. Zweifel).

https://doi.org/10.1016/j.compositesa.2023.107679
Received 6 January 2023; Received in revised form 26 April 2023; Accepted 4 July 2023
Available online 5 July 2023

triggers phase separation, and the cross-linking of epoxy, which freezes the structure and suppresses phase separation, leading to a semi-interpenetrating network (s-IPN) [4,12–15]. Different morphologies result from the reaction-induced phase separation, such as complete dissolution, a homogeneous distribution, sea-island structures, or a two-phase morphology, depending on the polymers, their mixing ratio, and the temperature condition [5,11]. Forming s-IPNs and phase-separating morphologies are essential mechanisms to improve fracture toughness [11]. This concept is interesting for toughening and designing multi-materials, e.g. integration of a functional surface in composite materials for welding [13,15–18], over-moulding [19], or as a sealing. Recent studies have demonstrated the usage of functional materials with favourable properties, including PES/epoxy [2,8], PEI/epoxy [5,14,15,20], poly hydroxy ether (phenoxy)/epoxy [6,17,18], poly (methyl methacrylate) (PMMA)/epoxy [18,21–23], thermoplastic elastomer (TPE)/epoxy [24], and polycarbonate/polyester resin [25].

Inspired by nature's ingenious designs, multifunctional materials have emerged as a promising avenue in composite materials research. Multifunctional materials refer to materials that exhibit multiple properties or functionalities, often beyond their traditional roles in a single material system, whereas multi-material materials refer to materials composed of different materials [26,27]. Multi-material materials focus on the combination of different materials, while multifunctional materials focus on the multiple functionalities exhibited by a single material [27]. By drawing insights from biological structures and processes, researchers develop composite materials that exhibit various functionalities, enabling clever and efficient structural designs without added weight or costs [26,27]. Bioinspiration in composite materials involves incorporating design principles observed in biological systems, such as hierarchical organisation, flexibility, and toughness, to create materials with enhanced mechanical properties and multi-functionality.

Bio-inspired composite materials have been explored in various engineering realms, ranging from robotics to life sciences, and have shown great potential in applications such as brittle-to-ductile toughening architectures [28,29], morphing structures [28,29], soft actuators [26,30–33], and beyond. The use of bioinspired approaches, including mimicking the helicoid features found in biomaterials [34,35] has shown promising results in creating multifunctional composite materials with improved performance and mechanical properties. Overall, the integration of bioinspiration in composite materials holds immense promise in advancing the field of multifunctional materials, paving the way for innovative and efficient structural designs with a wide range of applications.

This study aims to investigate the application of s-IPNswith pronounced mechanical interlocking at the micrometre scale [5,11] for integrating various functional regimes, including the mechanical functionality of a brittle-to-ductile material architecture, impact modification, and multi-scale toughening. The utilisation of s-IPNs allows for the combination of these functionalities, resulting in a synergistic effect that enhances the overall performance of the material system. This approach involves the creation of a complex network structure at the microscopic level, which provides mechanical interlocking between the different polymer networks, leading to improved mechanical properties, impact resistance, and toughening behaviour. By strategically designing the s-IPNs, it is possible to achieve tailored material properties that are superior to those of individual polymers or conventional composites. This study aims to provide a comprehensive understanding of the fundamental principles underlying the design and fabrication of s-IPNs for advanced materials with enhanced multifunctional performance, specifically by developing multifunctional materials based on brittle-to-ductile transition regions in epoxy-based composites formed by a gradient interphase with a bio-based TPE. TPE's combine the advantages of both rubbery and thermoplastic materials: high flexibility with the ability to be reshaped and formed through thermoplastic processes. The study proposes a workflow to design, manufacture, and assess multifunctional architectures, including characterising the interphase formation from bio-based Pebax®Rnew®35R53 and Pebax®Rnew®1100 with the fast-curing epoxy Araldite LY3585/Aradur 3475 via optical hot-stage microscopy and space-resolved Raman spectroscopy, as well as designing and manufacturing a composite laminate that combines the fused filament fabrication (FFF) process and the vacuum infusion process. The FFF-printed structure serves as a mould into which the fibre preforms are inserted, followed by infusion and curing of the epoxy. The resulting laminate exhibits different responses depending on the direction of applied load, showing pronounced flexibility in the bending direction and stiffness in the tensile direction. This is achieved by integrating a flexible domain with tailored variable stiffness properties, resulting in a brittle-to-ductile material architecture at the micrometre scale.

Table 1
Comparison of properties of different Pebax®Rnew types [38].

Property	Pebax®Rnew®35R53 [42]	Pebax®Rnew®1100 [43]
Amount of PA11	29 %	65 %
Melting temperature	135 °C	188 °C
Density	1020 kg/m^3	980 kg/m^3
Young's modulus	40 MPa	1160 MPa
Shore D hardness	25	68

2. Materials and methods

2.1. Materials

Two types of bio-based thermoplastic elastomers, Pebax®Rnew®35R53 and Pebax®Rnew®1100 (Arkema, Colombes, France), were used. The base material is beans of the castor plant, whereby the castor oil is converted into amino-11 monomers via several refinery steps [36]. The two types exhibit very different mechanical properties (see Table 1), from highly flexible to rigid. Pebax grades consist of a multi-block copolymer with two types of segments. The structure is a linear chain in an ordered pattern (AB) and consists of flexible polyether and rigid polyamide 11 (PA11) blocks. Hence, the crystalline polyamide block contributes to the polymer's thermoplastic behaviour, whereas the amorphous polyether block endows the polymer with elasticity and flexibility.

This study used an epoxy resin system (Araldite LY3585/Aradur 4375) provided by Huntsman Advanced Materials (Basel, Switzerland). The epoxy resin system (epoxy + hardener), hereafter referred to as the epoxy, is based on bisphenol-A-diglycidylether as the resin and 1,3-cyclohexanedimethanamine and methyldiethanolamine as hardeners. The system has been widely utilised in the mass production of automotive structural components and is notable for its short curing cycles and final glass transition temperature of approximately 120 °C. The system is typically used for high-pressure resin transfer moulding (HP-RTM), wet compression moulding, and dynamic fluid compression moulding (DFCM) applications, with a curing cycle of 2 min at 115 °C or 1 min at 140 °C. The DFCM process combines the speed of wet compression moulding with HP-RTM quality without sacrificing geometric complexity [33]. The authors previously developed a kinetic model using the modified Kamal–Sourour model to describe the curing process [18], and this model was used in this study to determine the degree of curing.

A glass-fibre fabric (twill weave, E-Glass, Finish FK-144 [37]) with an aerial weight of 163 g/m^2 was selected because it allows for better visual inspection of the sample after manufacturing and testing.

2.2. Optical hot-stage microscopy

A scientific optical hot-stage microscopy setup, similar to the one described by Teuwen et al. [13], was utilised for the microstructural analysis of thermoplastic films. The setup consisted of a controlled

Table 2
Experimentally derived parameters for Raman mapping.

Parameter	Value	Parameter	Value
Laser	638 nm	Hole	500 µm
Filter	15 mW (50 %)	Slit	100 µm
Lens	100×	Range	400–3500 cm^{-1}
Accumulations	5	Acquisition time	2 s
Grafting	600 (750 nm)	Delay time	0 s
Photobleaching	3 s	Binning	1
Autofocus mode	View Sharp™	Repetitive mode	Off

heating device (Linkam THMS600, Tadworth, Great Britain) coupled with an optical microscope (Keyence VHX 600, Osaka, Japan). The thermoplastic films were printed directly on cover glass using a Fused Filament Fabrication (FFF) technique on a Prusa i3 MK3S + 3D printer (Prague, Czech Republic). The films had dimensions of 7 × 24 mm^2, a slot of 3 × 20 mm^2, and a thickness of 120 µm, and the FFF parameters were adopted from Schär et al. [38]. The films were heated at a rate of 50 K min^{-1} above their respective melting temperatures (150 °C for Pebax®Rnew®35R53 and 230 °C for Pebax®Rnew®1100) to adhere the cover glass to the film. A toothpick was used to exert pressure and promote proper adhesion between the thermoplastic film and the cover glass. Subsequently, the temperature was gradually reduced to the predetermined curing temperature, ranging from 90 °C, 100 °C, 110 °C, 120 °C, 130 °C, and 140 °C, as per the experimental design. Upon reaching the curing temperature, a carefully prepared mixture of epoxy resin (Araldite LY3585) and amine hardener (Aradur 3475) was applied to the cavity. A time-lapse program captured images every 15 s to characterise the interphase.

2.3. Raman spectroscopy and scanning electron microscopy

The hot-stage specimens were prepared for thorough analysis using space-resolved Raman spectroscopy. A confocal Raman micro-spectrometer (Horiba XploRA™ PLUS, Kyoto, Japan) was employed to perform spectral mapping, enabling assessment of the interphase thickness and shape. The Raman mapping was conducted at each curing temperature, with the interphase thickness being measured three times to ensure accuracy and repeatability. The spatial resolution in the x and y directions was <500 nm, and that in the z direction was <2 µm; the spectral resolution (full-width at half-maximum) was 1.4–8 cm^{-1}, depending on the laser and grid. A 100× lens with a minimum working distance of 0.21 mm was used. Horiba's View Sharp™ software was used to reconstruct the surface topology to attain the highest focal quality and ensure robust measurements. The interphase mappings analysed via Raman spectroscopy were conducted using experimentally determined parameters, as outlined in Table 2. The chosen parameter set was found to be suitable for both Pebax®Rnew®35R53 and Pebax®Rnew®1100 grades. Different mapping grids were employed for the two grades due to the significant difference in interphase thickness. For Pebax®Rnew®35R53, mappings were acquired with a size of 400 × 42 $µm^2$, with step sizes of 0.9 µm and 14 µm in the x- and y-directions, respectively, resulting in 445 spectra per row and column. For Pebax®Rnew®1100, mappings were acquired with a size of 170 × 30 $µm^2$, with step sizes of 0.5 µm and 10 µm in the x- and y-directions, respectively, resulting in 340 spectra per row and column. The resulting Raman spectra were processed to generate false colour images that visualised the material change in the interphase area (see Fig. 1). Instead of false colour representation, normalised concentration profiles were used in the x-direction to reveal the concentration gradient. Two rigorous statistical methods were employed to analyse the experimental data. Firstly, the interphase thickness was determined by comparing the

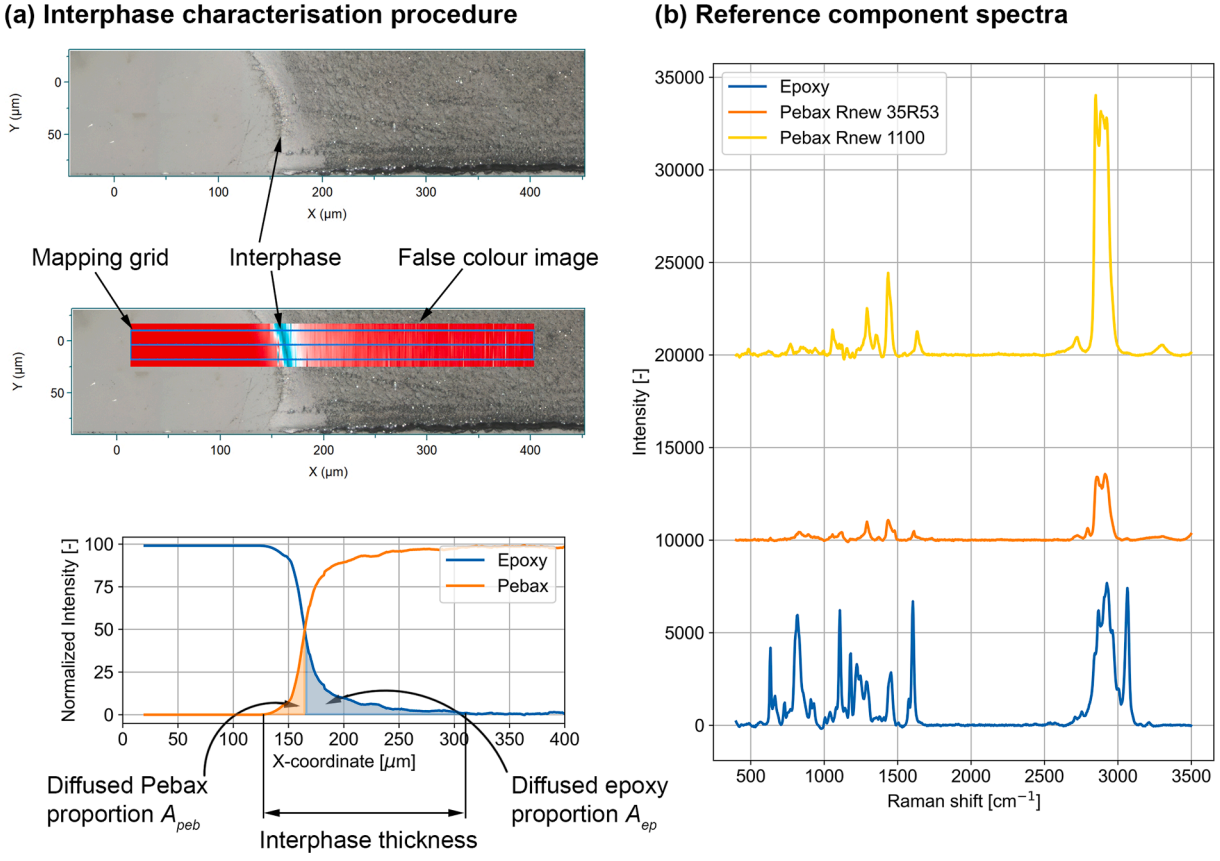

Fig. 1. Measurement and analysis setup for spectral Raman mapping to quantify the thickness, shape, and diffused proportions of interphases.

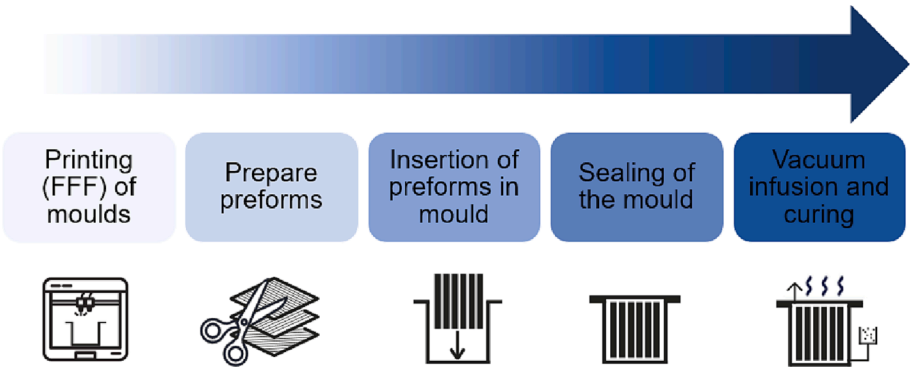

Fig. 2. Manufacturing concept combining fused filament fabrication (FFF) with a vacuum infusion process (adapted from [39]).

onset and termination points, as depicted in Fig. 1. Secondly, the integral of the diffused proportions within these boundaries was calculated, enabling quantification of the rate at which diffusion occurred between the two materials. The ratio R was defined as

$$R = \frac{A_{ep}}{A_{peb}}, \tag{1}$$

whereby A_{ep} is the integrated diffused proportion in the epoxy and A_{peb} is the integrated diffused proportion in the Pebax (see Fig. 1). The data

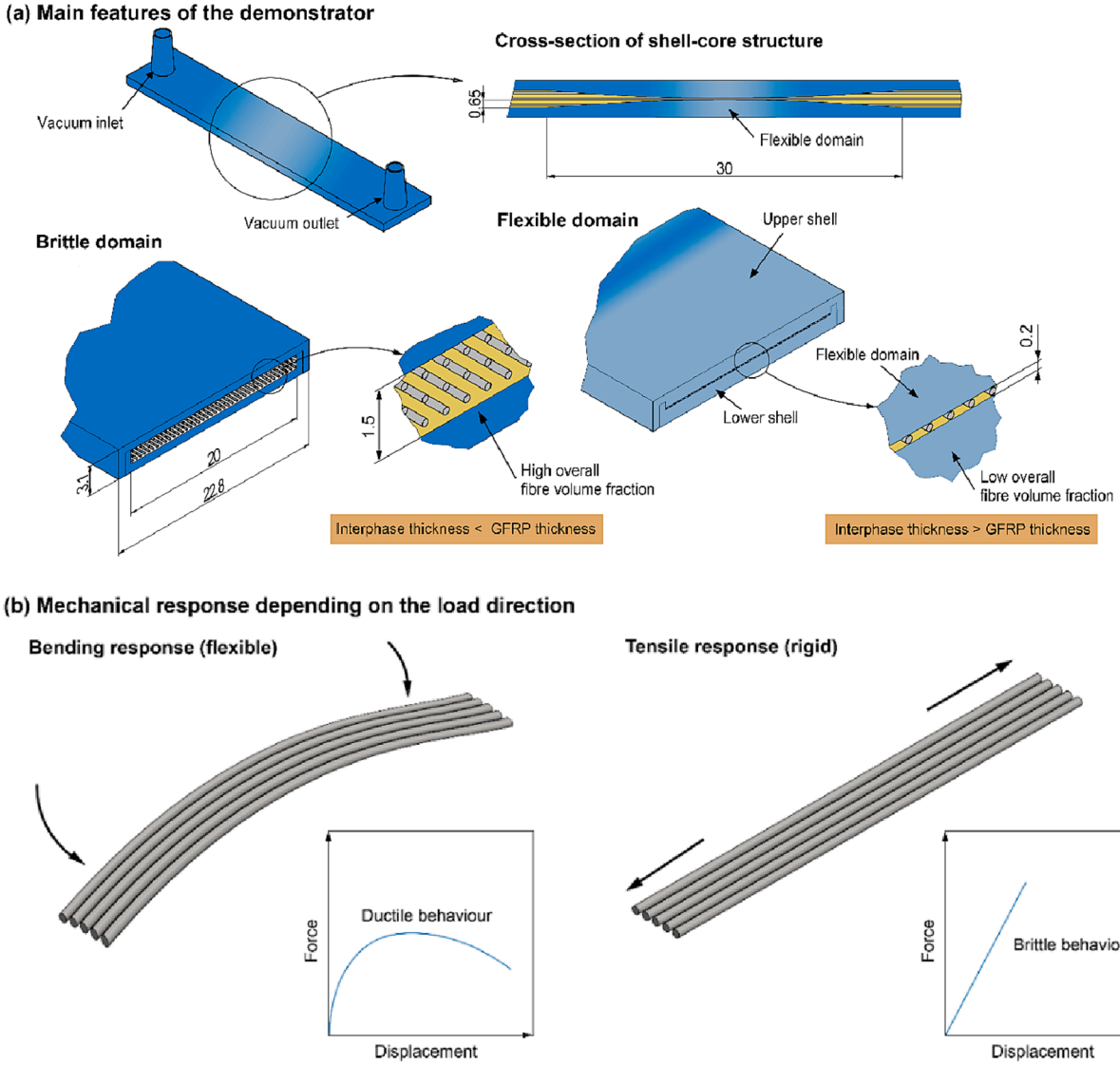

Fig. 3. Overview of key aspects of the multifunctional composite laminate: (a) Main features of the multifunctional composite laminates; (b) Mechanical response depending on the loading direction.

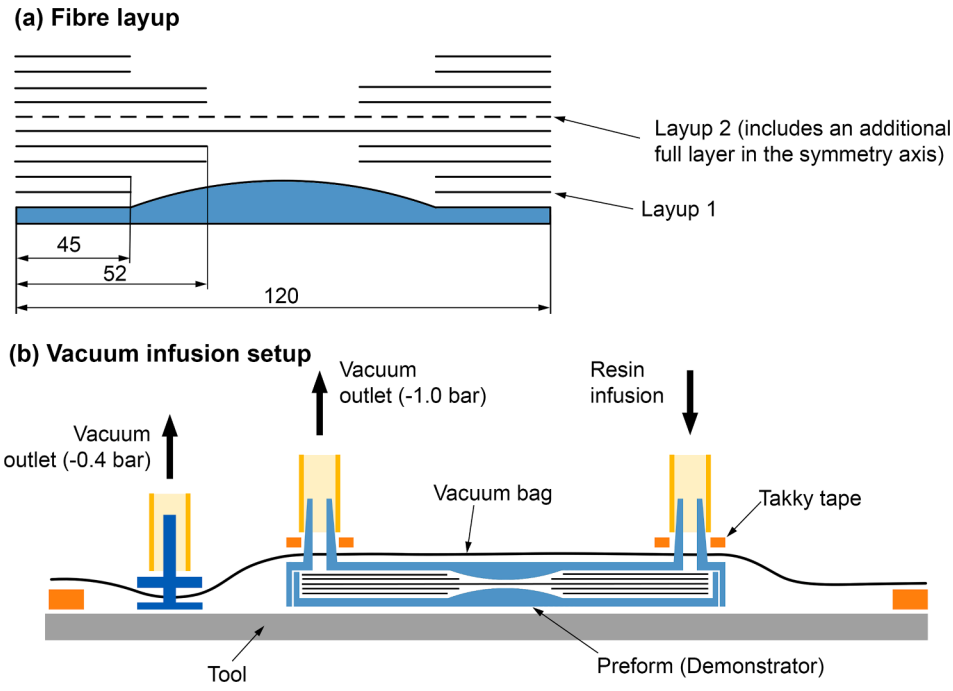

Fig. 4. Schematic representation of the fibre layup in the combined fused filament fabrication (FFF) with vacuum infusion process for manufacturing laminates with fibre composite structures.

analysis of the measured spectra was performed using LabSpec6 software (Version 6.5.1, Horiba, Kyoto, Japan). First, a baseline correction was performed. Second, the spectra were analysed: despite the possibility of using individual peak signals to derive the concentration gradient between the two materials, the multivariate classical least squares (CLS) toolbox was used for the analysis. The CLS Fitting toolbox is a supervised multivariate decomposition technique that uses a set of reference component spectra. This procedure was used to calculate the contribution of reference spectra within the acquired mapping grid and allowed a quantitative evaluation of the interphase thickness.

Scanning electron microscopy (SEM; Hitachi S-3400, Tokyo, Japan) was used on the identical specimens to obtain a more detailed view of the interphase between the epoxy and Pebax. The samples were analysed with and without etching before measurement in order to resolve the microstructure of the gradient interphase. The etching was performed with hexafluoropropane-2-ol for 1–10 min followed by rinsing with ethanol and with distilled water and drying with compressed air.

2.4. *Manufacturing of composite laminates with a brittle–to–ductile material architecture*

This study combined FFF with a vacuum infusion process to manufacture specimens with fibre composite structures. The FFF process allows for design freedom through the inclusion of a flexible domain, whereby the local stiffness and elasticity can be modified according to the specific needs and requirements; moreover, it also allows for manufacturing without a mould [37]. Thus, this concept allows for composite designs close to the final contour near the net shape [38,39]. A shell structure consisting of two parts was printed via FFF; the dry glass-fibre fabrics were inserted and subsequently impregnated through vacuum infusion followed by curing with the epoxy system in an oven (see Fig. 2).

During the infusion process, the reaction–diffusion behaviour of the epoxy ideally creates a pronounced gradient interphase between the shell and the core. Previous studies have shown that in addition to simple interlayers [13,14,20], multiple film stackings are possible, in which multiple interphases are apparent [7]. Hence, the scale of the brittle-to-ductile architecture formed by multiple gradient interphases and neat polymer domains is passively tailored by design. The chosen design for this study allows a high stiffness in the tensile direction with a flexible flexural response in the bending direction (see Fig. 3). The flexible domain was designed with a thickness of 0.2 mm, implying that after curing, most of the infused epoxy eventually formed an interphase with the TPE, and thus leading to a fully gradient material without brittle epoxy properties. Nevertheless, this hypothesis needs to be verified through hot-stage microscopy, Raman spectroscopy and mechanical tests.

In total, six composite laminates were manufactured with two types of fabric layup (L1, L2). The L1 and L2 layups consisted of nine and ten individual fabric layers, respectively. The fibres were oriented in the tensile direction, which made it possible to produce a structure consisting of a form-giving shell and a load-bearing core composed of glass-fibre reinforcement and epoxy resin. The layup was designed so that the centre layers entirely covered the mould area; all other layers were adapted to the flexible domain in the centre (see Fig. 4a). The main difference between layups L1 and L2 was an additional UD-laminae in the centre to demonstrate the effect of the architecture on the mechanical properties. The outer shell was printed from Pebax with the FFF printing parameters given in [38] and a size of 22.8 × 120 × 3.1 mm^3 which was co-bonded with the glass fibre-reinforced epoxy system in a vacuum infusion setup (see Fig. 4b).

After curing, the specimens were evaluated in three steps: 1. visual inspection and proof of concept; 2. micro-polished cross-sections (qualitative); and 3. quantitative mechanical in a Zwick (Zwick Roell, Ulm, Germany) universal tensile testing machine according to DIN EN ISO 178 (flexural mode) and DIN EN ISO 527 (tensile mode). The strains were measured via the traverse. The flexural response was measured with a 1 kN load cell and a three-point bending setup comprising a span length between the supports of 64 mm, a radius of the support and leading edge of 5 mm, and a testing speed of 5 mm/min. The tensile properties were measured with a 100 kN load cell via hydraulic clamping jaws with a pressure of 25 bar and a testing speed of 2 mm/min. Subsequently, microsection analysis of the composite part were performed. From each laminate, several samples were removed for

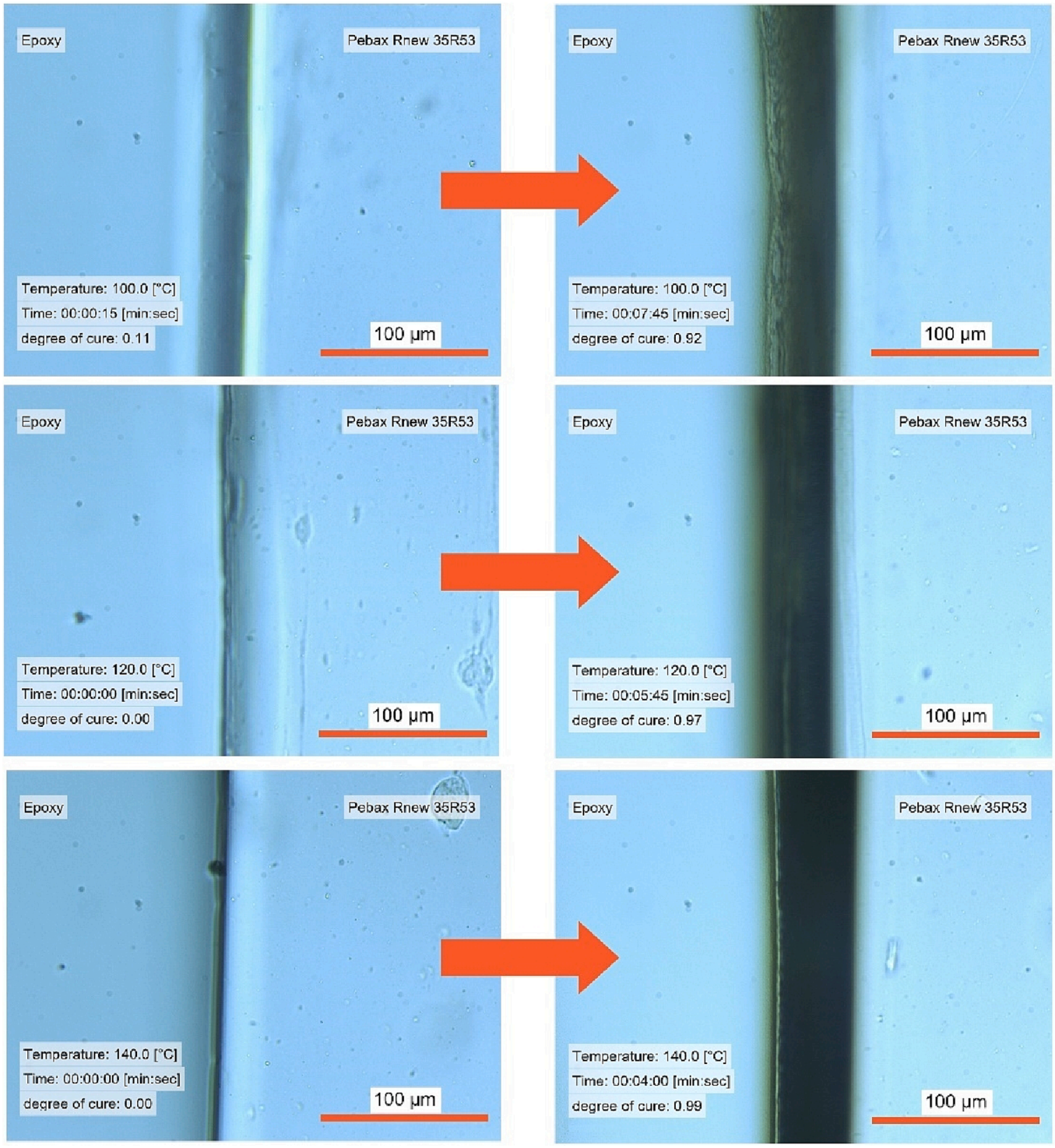

Fig. 5. Optical hot-stage microscopy images of the Pebax®Rnew®35R53 and epoxy system LY3585/3475 at 100 °C, 120 °C, and 140 °C. The left image illustrates a degree of curing of zero, while the right image displays the maximum degree of curing.

polishing and microscopy.

3. Results and discussion

3.1. Interphase formation

Fig. 5 displays two images, captured at different curing temperatures, that depict the progressive stages of the curing process. The left image represents the initial stage when the epoxy was introduced into the cavity, while the corresponding image on the right illustrates the maximum degree of curing, clearly highlighting the interphase formed between the thermoset and thermoplastic materials. Optical hot-stage microscopy was employed to investigate the interphase formation mechanisms owing to the notable mobility and affinity of both Pebax®Rnew® grades towards the epoxy. Despite the hindrance posed by the fast-curing reaction, which limits the evolution of the interphase, distinct reaction–diffusion phenomena were observed. In comparison, other thermoplastic materials such as polyamide 12, PMMA, and

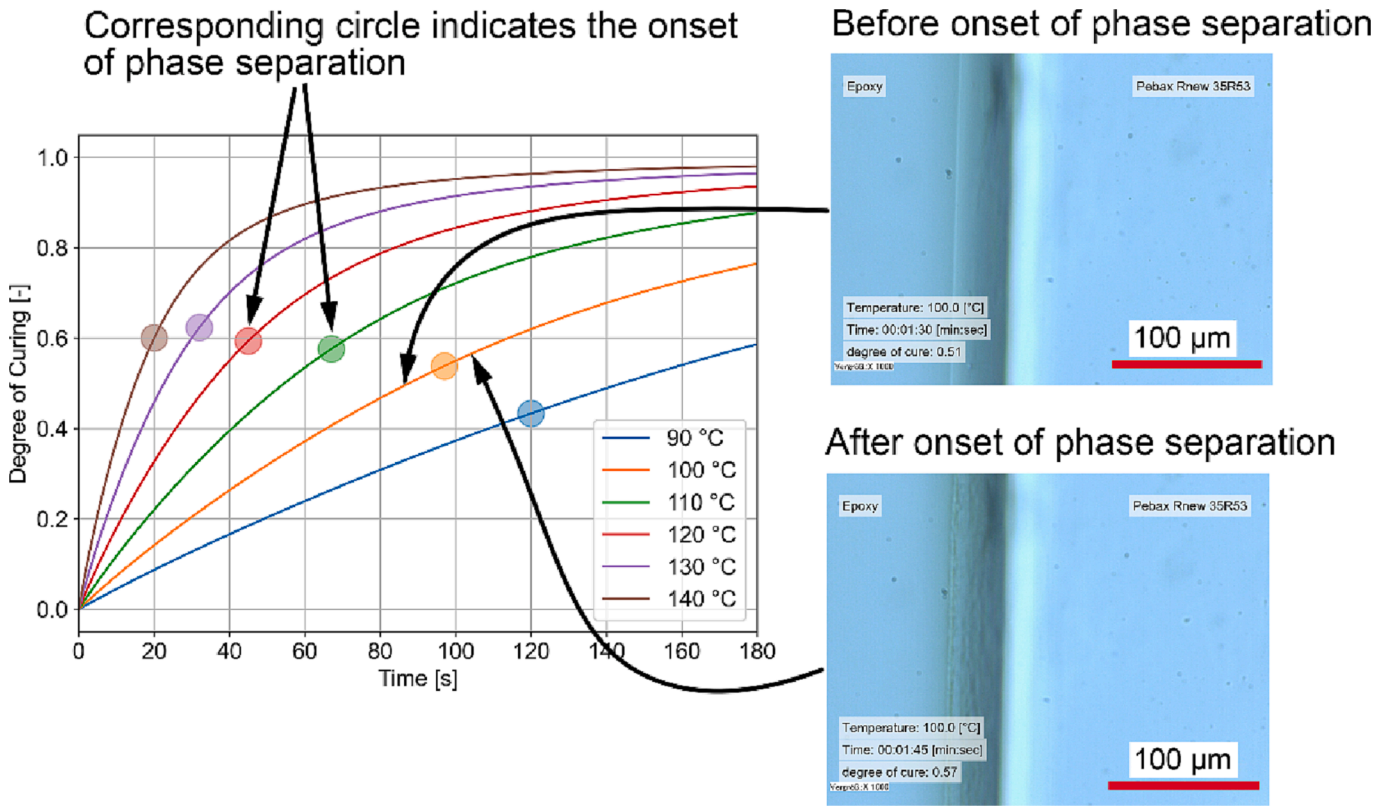

Fig. 6. Isothermal cure kinetics of the epoxy system Araldite LY3585/Aradur 3475 [18] with the corresponding onset of phase separation timesteps from Pebax®Rnew®35R53.

phenoxy exhibited comparatively lower diffusion rates, as reported in previous studies [18]. The Pebax®Rnew®35R53/epoxy exhibited pronounced interphase formation mechanisms comparable to the formation mechanisms observed in but not limited to PEI/epoxy investigations [5,13,15,18,20,40]. Consequently, a concentration gradient of the two constituents was formed, as visually indicated by the darkish area in Fig. 5. The occurrence of dissolution, swelling, and interdiffusion was confirmed, albeit with moderate levels of prominence. The initiation and completion of the phase separation process were distinctly identified in the conducted tests based on alterations in the refraction index and colour. The onset of phase separation was visually apparent through the decomposition of constituents at the diffusion front on the left-hand side (see Fig. 6). The phenomenon of reaction-induced phase separation is observed when the concentration of reaction products surpasses a critical threshold, resulting in the formation of one or more distinct phases from a previously homogeneous mixture. Fig. 6 displays the cure kinetics of the reaction along with the onset of phase separation information represented by circles on the dedicated curing curve. It is important to note that higher temperatures delay the onset of phase separation in this system similar to [13], typically before the gelation in the epoxy-amine system is initiated [41]. Nonetheless, the formed interphase exhibited predominantly dark colours, owing to changes in the refraction index during the curing process. Therefore, determining the interphase thickness from hot-stage experiments is not straightforward, and a comparison of various methods can be found in reference [14]. However, it was observed that the interphase thickness was estimated to be approximately 40–60 µm, suggesting a comparatively rapid diffusion rate during the curing process in comparison to the other systems mentioned [18]. The Pebax®Rnew®1100/epoxy composite material demonstrated a lower degree of affinity with the epoxy system in contrast to the Pebax®Rnew®35R53/epoxy composite (see Fig. 7), attributable to its relatively slower diffusion rates and correspondingly smaller final interphase. Consequently, the extent of thermoplastic diffusion during the curing process was found to be dependent on the PA11 concentration in the Pebax grade. This observation could be attributed to the increased free volume of the amorphous flexible polyether, promoting notable dissolution and diffusion of the epoxide or amine hardener monomers. The rigid PA11 segments, which form a semicrystalline structure through hydrogen bonding (see Fig. 8), exhibit limited molecular mobility. As the polyamide content in Pebax®Rnew®1100/epoxy composite increases from 29 to 65 %, its impact on the mobility of the composite during interphase formation can be quantitatively measured. This is evidenced by a decrease in mobility. Furthermore, the observed colour change and decomposition occurring at the epoxy-rich side of the interphase provide potential evidence of phase separation between the polyamide and epoxy components. The high reactivity of the epoxy system, combined with the small interphase thicknesses, resulted in the inability to characterise the onset of phase separation. This is because all physicochemical effects were rapidly quenched within a small spatial timestep. The estimated thickness of the interphase, ranging from approximately 20 to 30 µm, suggests that the increased polyamide content results in a lower diffusivity, indicating reduced molecular movement across the interphase boundary.

For the Pebax®Rnew®35R53/epoxy, as seen in the hot-stage experiments, increased molecular mobility already occurs at the lowest temperature (see Fig. 9). The spatial Raman concentration profiles show that Pebax®Rnew®35R53 does not diffuse significantly into the epoxy compared to the diffusion from the epoxy into Pebax®Rnew®35R53, which is visible through the steep concentration drop. Thus, the apparent change in concentration exhibits a much faster change than existing interphase measurements [13,14,18]. The epoxy exhibits a noticeable penetration into the Pebax®Rnew®35R53 material, as evidenced by the smooth and elongated concentration change observed towards the Pebax®Rnew®35R53 matrix. As mentioned earlier, the Pebax®Rnew®35R53 matrix incorporates significant free volume, providing space for the diffusion of the epoxy and amine monomers.

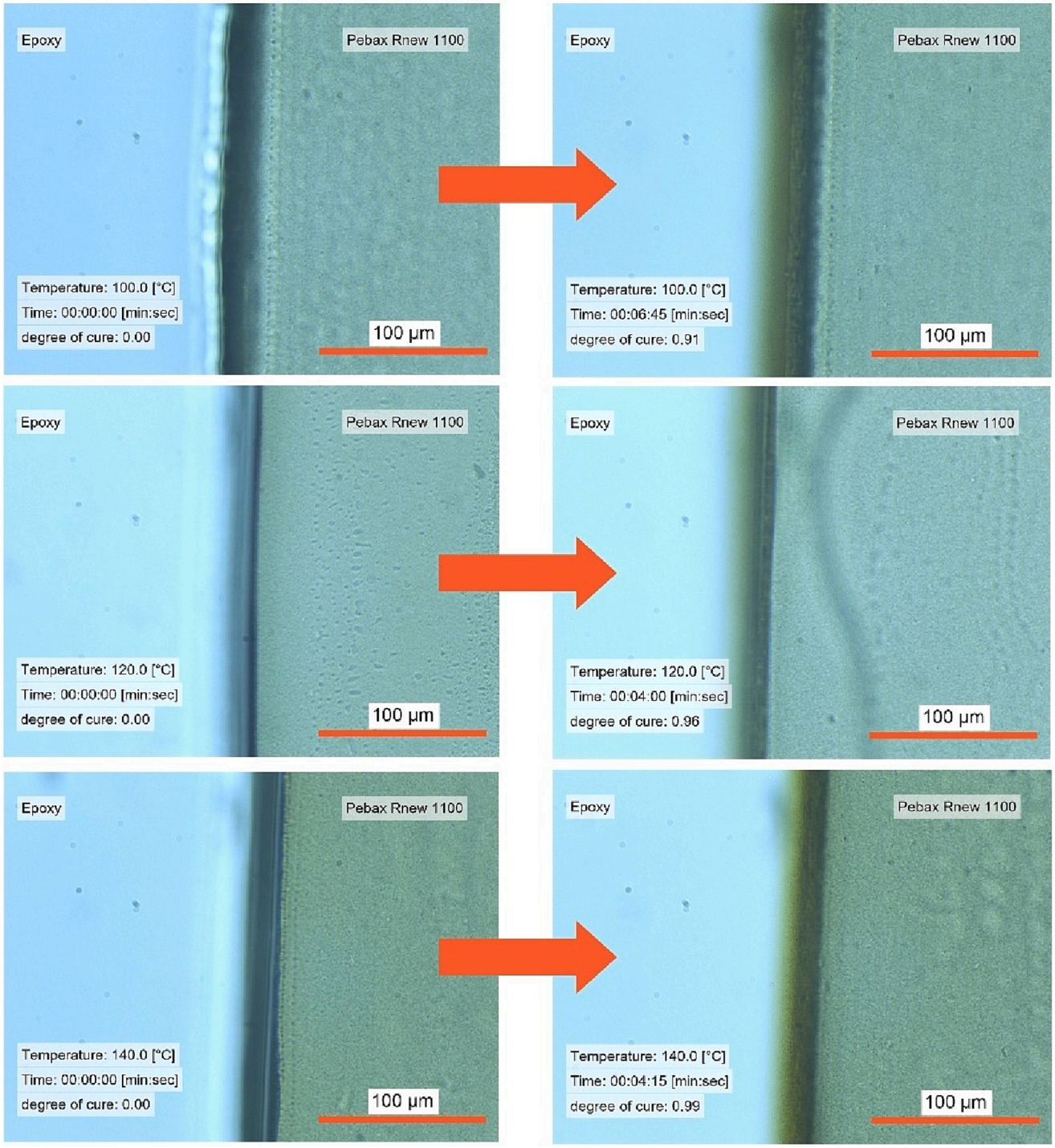

Fig. 7. Optical hot-stage microscopy images of the Pebax®Rnew®1100 and epoxy system LY3585/3475 at 100 °C, 120 °C, and 140 °C. The left image depicts a degree of curing of zero, while the right image exhibits the maximum degree of curing.

Notably, when a higher curing temperature is employed, the concentration drop becomes smoother, which is expected as the epoxy exhibits enhanced solvent-like behaviour at elevated temperatures, facilitating greater mobility and diffusion within the matrix. As soon as the epoxy system reaches the gel point, the molecular weight starts to increase rapidly, whereas the reaction speed of the epoxy surpasses its diffusion speed, and no further increase of the interphase thickness can be achieved. Fig. 10 shows the resulting interphase thickness results depending on the curing temperature. A maximum interphase thickness of 219 µm (±2.4 %) was achieved with a curing temperature of 120 °C. The maximum interphase thickness corresponds to an optimum value within the related curing cycles of the epoxy system. The observed variability in thickness measurements were attributed to diverse geometric effects such as fluctuations in cutting edges, presence of impurities within the diffusion front, and local heterogeneities in the multi-component system, such as variations in epoxy/amine mixing ratio.

The interphase thickness of the Pebax®Rnew®1100/epoxy system is reduced compared to that of the Pebax®Rnew®35R53/epoxy system, as revealed by concentration mappings. Minimal diffusion from the epoxy to the Pebax®Rnew®1100 is observed, even at an elevated temperature

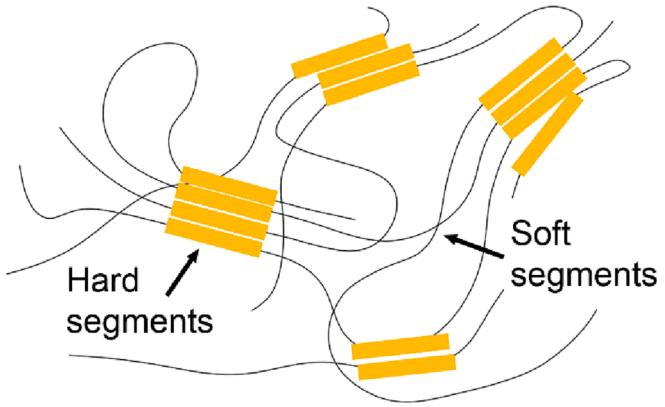

Fig. 8. Representative structure of Pebax copolymers featuring hard PA11 segments and soft segments.

of 140 °C. Therefore, it can be concluded that the polyamide part (67 % in this grade) of the copolymer ultimately hinders diffusion between the Pebax®Rnew®1100 and epoxy, resulting in low interphase thicknesses. Despite this, a more pronounced interphase was observed compared to other polyamide diffusion studies, which show that polyamide rarely diffuses at high rates [18]. A maximum interphase thickness of 34 µm (±6.54 %) was achieved at a curing temperature of 140 °C (see Fig. 10). The maximum interphase thickness does not correspond to an optimum value within the related curing cycles of the epoxy system.

As the next post-processing step, the ratio *R* (see equation (1) was compared for the epoxy system diffused into the Pebax and vice versa (see Fig. 1). Fig. 11 presents the resulting ratios as a function of curing temperature. In the case of Pebax®Rnew®35R53/epoxy, the qualitative assessment was corroborated, revealing an increase in the diffused proportion of Pebax®Rnew®35R53 with higher curing temperatures, leading to a decrease in the ratio *R*. Notably, the ratio of diffused epoxy with Pebax®Rnew®35R53 at lower temperatures was nearly four times higher. Nevertheless, the comparison of the diffused proportion in the Pebax®Rnew®1100/epoxy system did not exhibit similar trends, which can be attributed to the increased variance and smaller magnitude observed in the interphase thickness measurements. Further investigation and characterization are necessary to comprehensively understand and interpret the observed differences in the proportions of diffused species between these two systems.

Subsequently, the interphase specimens were subjected to SEM analysis, with an exclusive focus on the Pebax®Rnew®35R53/epoxy system. Three distinct states were examined: unetched, etched for 1 min, and etched for 10 min with hexafluoropropane-2-ol. The results, presented in Fig. 12, revealed intriguing findings. Firstly, the unetched samples exhibited diverse morphologies across the interphase thickness, with small precipitates observed on the left-hand side, gradually increasing in size and shape towards the right end of the image. Secondly, both etched images displayed etching of the pure component of Pebax®Rnew®35R53, providing further insights into the interphase characteristics. Nevertheless, the interphase persists and exhibits notable precipitates of the phase-separated morphology. The interphase seems to dismantle from the pure epoxy component on the left. The degree of detachment increases after 10 min of etching. Therefore, it appears that the weakest connection of the interphase occurs at the beginning of the interphase to the epoxy.

3.2. Evaluation of the composite laminates

A total of six specimens (three samples of each of layup L1 and L2) were manufactured using Pebax®Rnew®35R53 as the selected material for the 3D-printed outer shell. This choice was based on its increased diffusivity and maximum interphase thickness observed at a curing

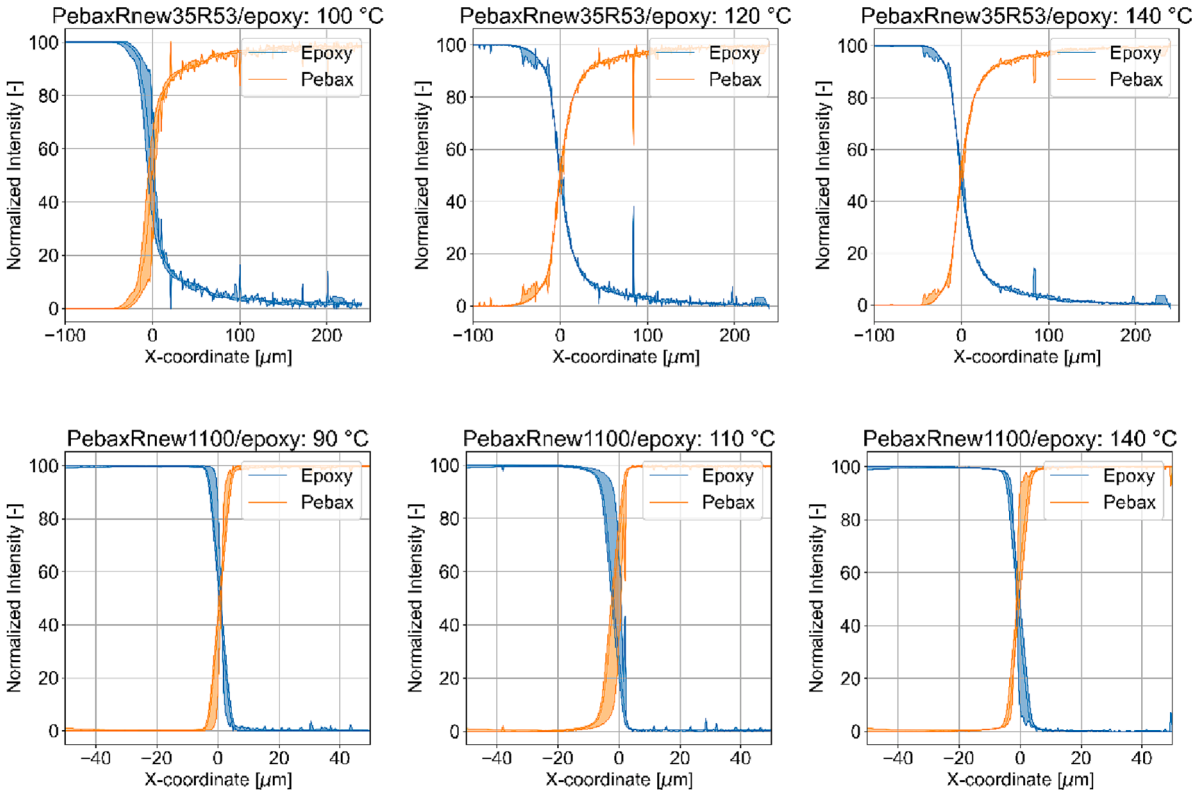

Fig. 9. Interphase measurements as a function of curing temperature: (top row) Concentration profiles obtained using the Raman CLS Fitting toolbox for Pebax®Rnew®35R53/epoxy specimens cured at 100 °C, 120 °C, and 140 °C; (bottom row) Concentration profiles obtained using the Raman CLS Fitting toolbox for Pebax®Rnew®1100/epoxy specimens cured at 90 °C, 110 °C, and 140 °C.

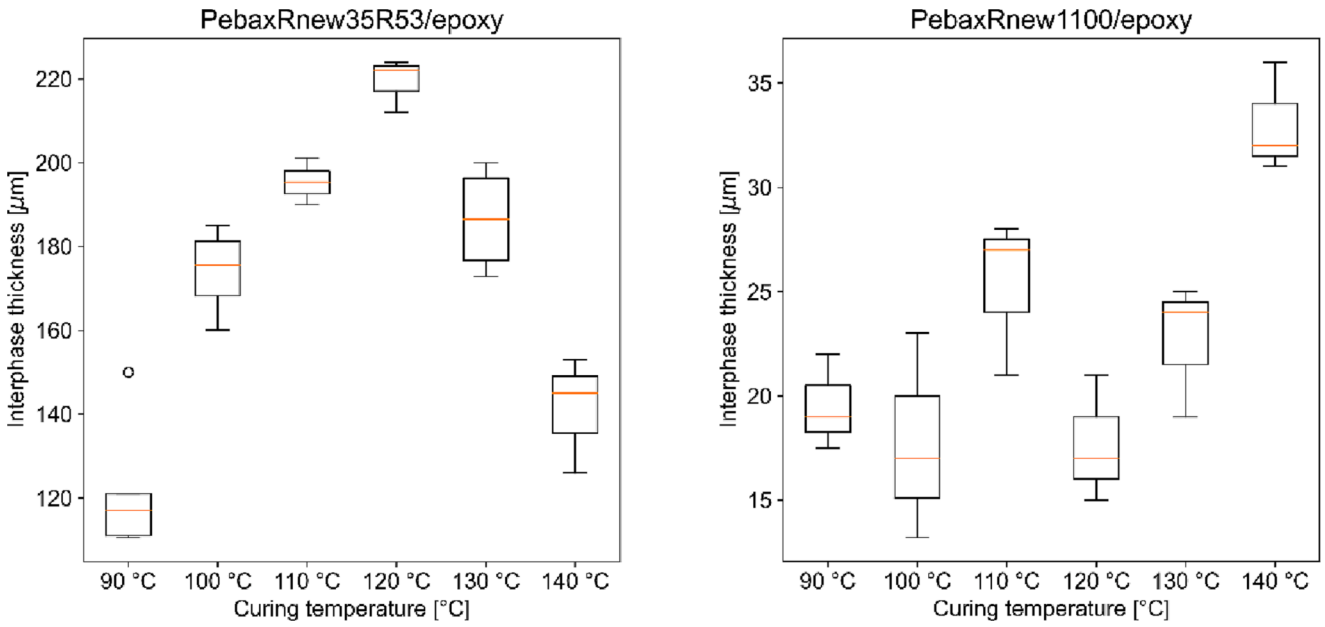

Fig. 10. Interphase thickness as a function of curing temperature: (left) Pebax®Rnew®35R53/epoxy interphase thickness, and (right) Pebax®Rnew®1100/epoxy interphase thickness.

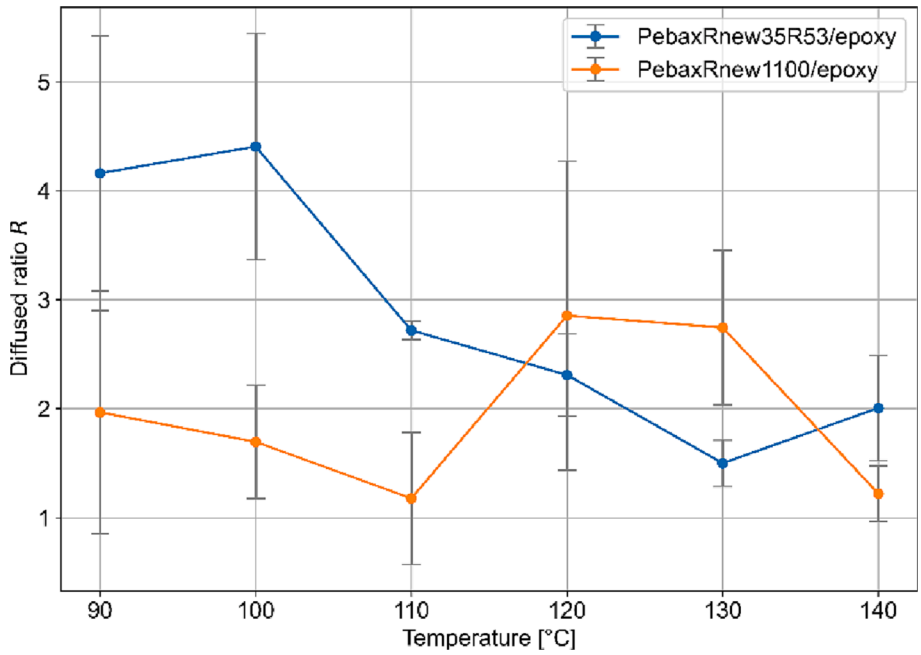

Fig. 11. Ratio of the integrated diffused proportions in epoxy and Pebax, as determined from Raman mappings acquired at the measured curing temperatures.

temperature of 120 °C. After several iterations, the composite manufacturing procedure was optimised, which consisted of the following steps: (1) printing of the shell structure (mould) composed of an upper and lower part with vacuum inlets and outlets according to the parameters provided in [38]; (2) cutting of the glass fibre layers; (3) hand layup of the fabric preforms into the mould; (4) closing the mould by combining both shell elements; (5) insertion of the mould into a vacuum setup and embossing of the two shell elements for 4 min at 140 °C (note that the embossing process does not result in perfectly fused shell elements); (6) sealing the mould; (7) gluing the vacuum inlet and outlet; (8) checking the leak-proofness at < 10 mbar/min through measurement of the vacuum loss before and after the mould; (9) preparing 35 g of epoxy resin and degassing at room temperature for 30 min; (10) placing the laminate in the layup configuration as shown in Fig. 4; (11) preheating the oven to 120 °C and installing the vacuum setup in the oven; and (12) mixing the epoxy resin, infusing, and curing for 5 min.

Fig. 13 illustrates the key features of the flexible zone, where the multifunctional architecture allows for elastic deformation in the bending direction and stiff behaviour in the tensile direction, along with the presence of a multi-material gradient. Bending up to 90° does not initiate cracks in the flexible zone, indicating its durability. Furthermore, the printed mould structure presents an ideal impact-resistant shell surrounding the fibre-reinforced composite. Subsequently, micro-polished cross-sections were used to evaluate the quality of the manufactured samples and control the topologies, as depicted in Fig. 14. The

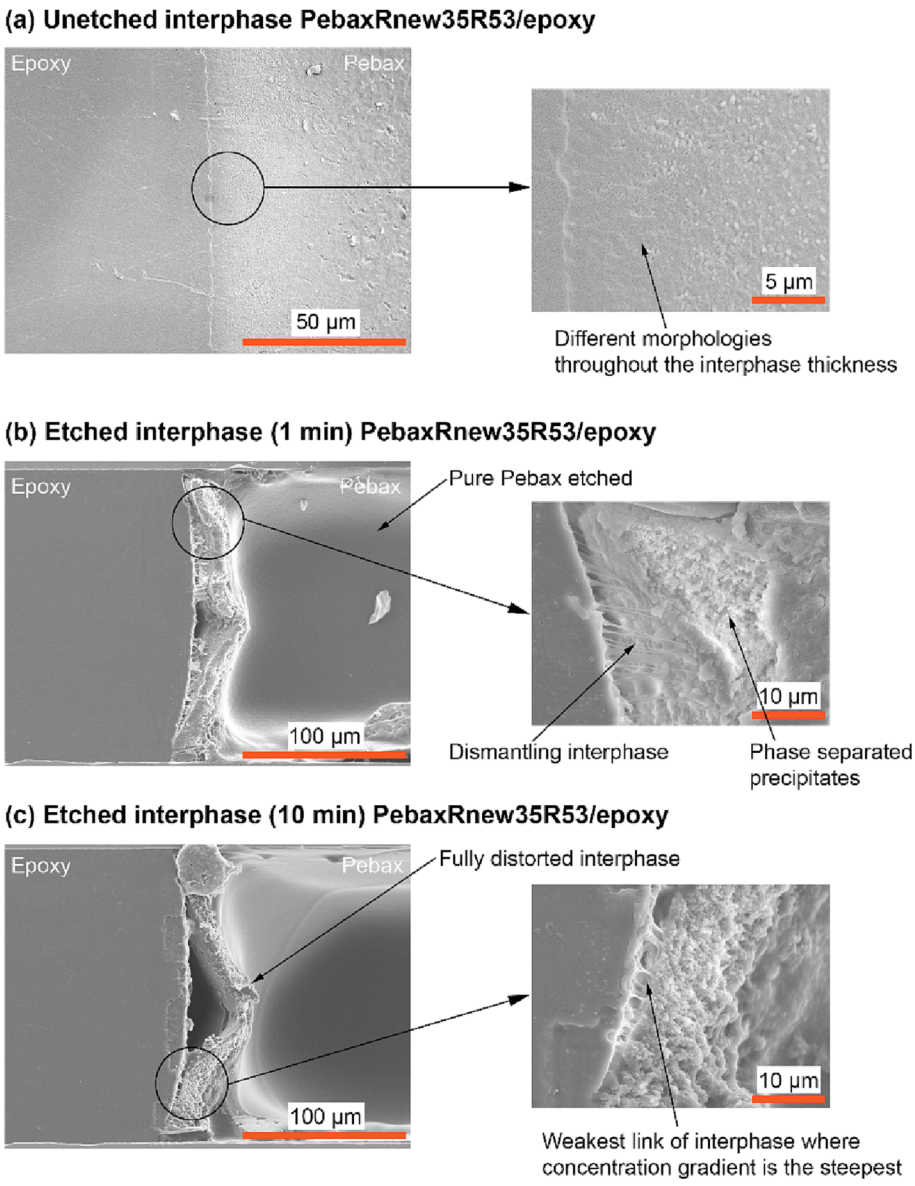

Fig. 12. Micro-polished cross-section of the Pebax®Rnew®35R53/epoxy interphase, showing the effects of different etching durations: (a) No etching; (b) 1 min of etching; (c) 10 min of etching.

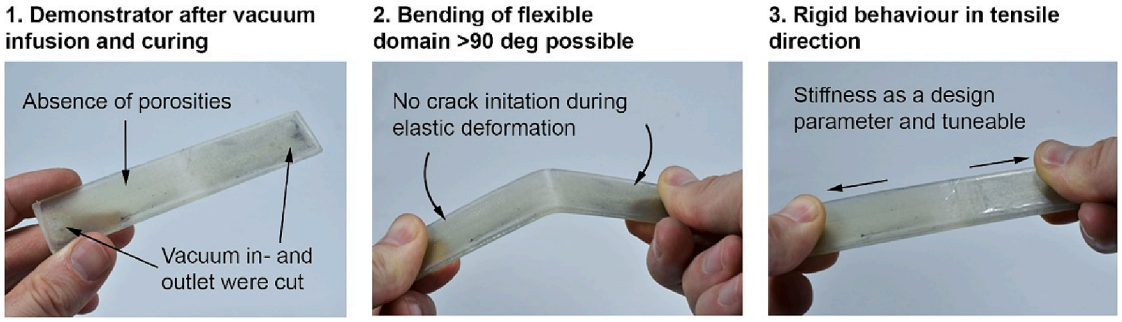

Fig. 13. Visual inspection of the multifunctional composite laminate showcasing its essential functional properties: mechanical functionality, multi-scale toughening, and impact resistance.

microsections were analysed in both brittle and flexible domains. The Pebax component, depicted in black colours, can be observed surrounding the epoxy composite. The vacuum infusion process demonstrated favourable results as the epoxy polymer filled the cavity without visible pores or dry spots, validating the successful application of printing a mould and then sealing it. The interphase between the epoxy and Pebax is visible, with a measured thickness ranging from 80 to 130 µm, proving the concept of multi-scale toughening. However, it should

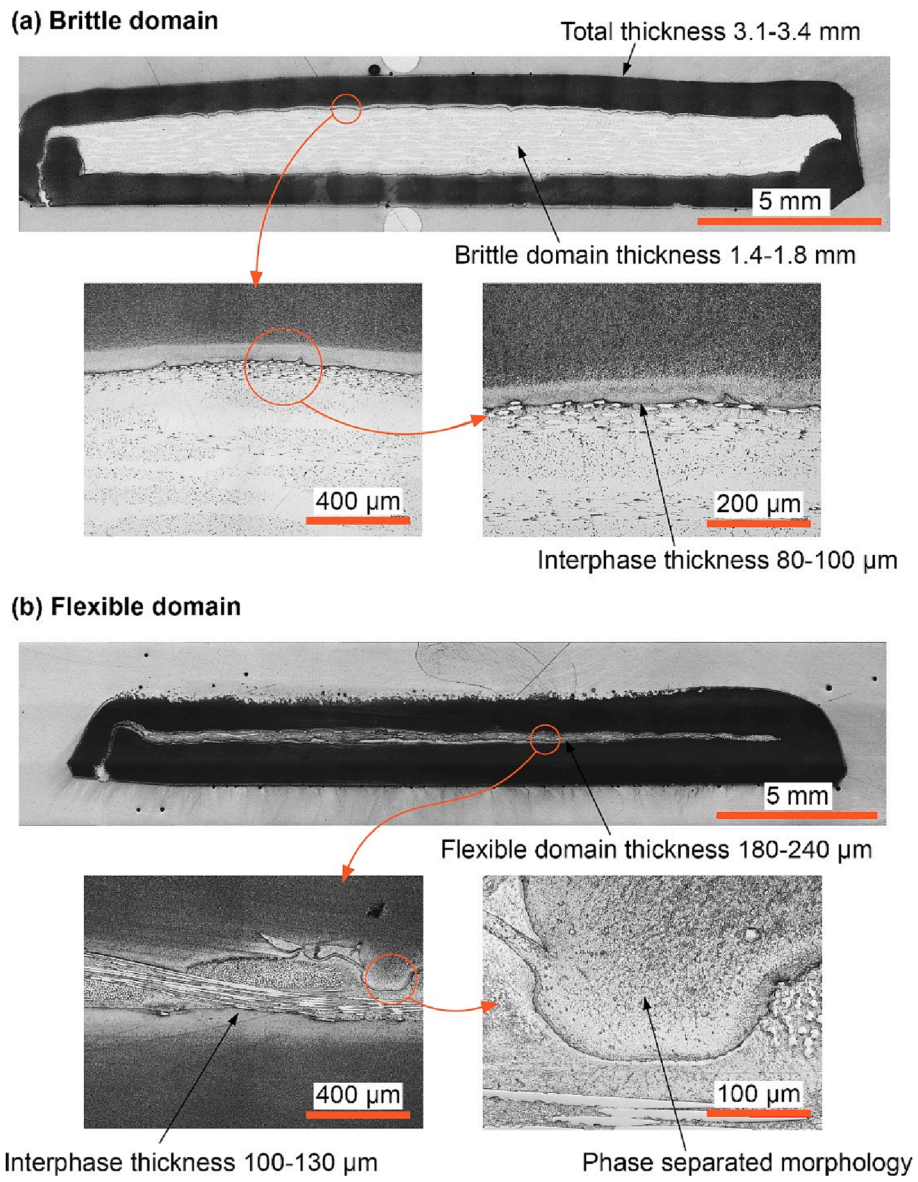

Fig. 14. Micro-polished cross-sections of the Pebax®Rnew®35R53/epoxy specimen with layup L1.

be noted that optical measurements tend to underestimate the actual interphase thickness, as evident from the comparison of optical and spectral measurements conducted in this study. To achieve higher measurement accuracy, three Raman mappings were conducted, yielding an average interphase thickness of 192 µm ± 10.6 µm. As reported in a recent study, this thickness is 11 % lower than the interphase thickness observed in the hot stage experiments (219 µm). The reduction in interphase thickness due to fibre reinforcement is consistent with the study's findings [24], which identified the composite architecture as a hindrance to diffusivity. The laminates exhibit a total thickness ranging from 3.1 to 3.4 mm, with a planned thickness of 3.1 mm. The epoxy composite component ranged from 1.4 to 1.8 mm, with a targeted thickness of 1.5 mm. The observed differences in thickness can be attributed to elastic deformation of the Pebax material during the layup and vacuum infusion processes. In the flexible domain, the composite region was anticipated to have a thickness of 200 µm, with the actual thickness of the fibre ply ranging from 180 µm to 240 µm. Therefore, the measured interphase thickness of 219 µm at 120 °C suggests that the pure epoxy regime was fully dissolved by the Pebax component, resulting in a fully ductile material architecture. The measured interphase thickness in the flexible domain is slightly higher than in the brittle domain, which can be explained by the less prominent presence of fibres, as previously stated [24].

In the third step, the mechanical performance under tensile and bending loading was tested, as described in Section 2 (see Fig. 15). First, the flexural properties were evaluated; it was possible to observe that the sample behaved like a hinge with a low bending force. It was possible to deform the sample up to an angle of 94° (equal to 30 mm deformation), confirming that the concept of a flexible region is applicable. The maximum displacement did not result in the maximum force: For L1, the maximum force of 18 N was reached at a deflection of 11 %; for L2, the maximum force of 15.6 N was reached at a deflection of 13 %. The samples were then tested in a modified tensile test to evaluate the mechanical performance. Different methods were used to evaluate the failure stress of the sample based on the cross-section of the complete specimen (3.1 × 20 mm^2) or the cross-section in the ductile domain (0.2 × 20 mm^2). The peak force for L1 was 1049 N with a standard deviation of 62 N (5.9 %), whereas the peak for L2 was 1825 N with a standard deviation of 84 N (4.6 %). The force–displacement diagram of the tensile test in Fig. 15 exposes for L2 (orange curve) a change from elastic to plastic deformation: The curve initially indicates a linear elastic behaviour up to 1100 N. From 1100 N up to the maximum load, the line

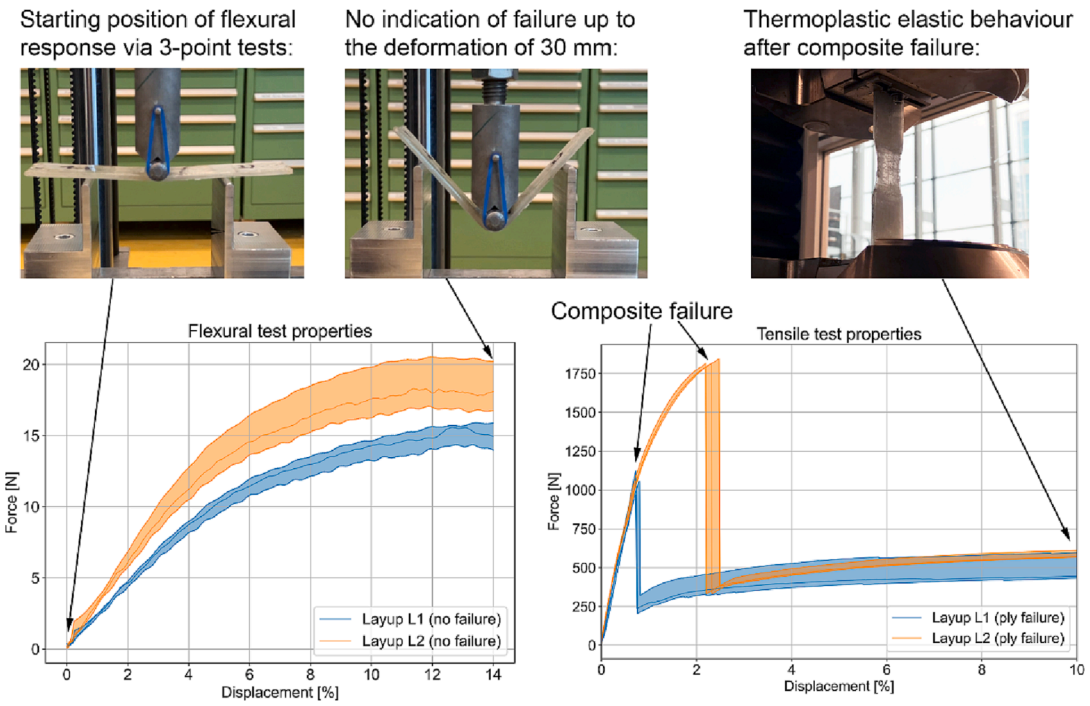

Fig. 15. Mechanical characterisation of specimens with fibre layups L1 and L2 through flexural and tensile testing.

Table 3
Mechanical properties of the composite laminate with brittle-to-ductile architecture.

Layup	Peak force [N]	Complete cross-section		Ductile composite cross-section	
		Area [mm^2]	Tensile strength [MPa]	Area [mm^2]	Tensile strength [MPa]
L1	1049 +/- 62	3.1 × 20	16.9 +/- 1	0.2 × 20	262.3 +/- 15.5
L2	1825 +/- 84	3.1 × 20	29.4 +/- 1.4	0.2 × 20	456.3 +/- 21

gradually flattens out, meaning a decrease in tensile stiffness. L1 (blue curve) follows the same trend as L2, but only in its (lower) elastic regime. The (upper) plastic deformation part of the curve appears to be cut off. This solely linear-elastic load–displacement curve would align with this study's topology concept: The single UD-laminae at the centre of the L1 coupon features a linear-elastic stress–strain relationship up to failure, as it can be expected from common glass-fibre reinforced polymer UD-laminates under quasi-static tensile loading conditions. L2 contains two central UD-laminae instead of one in L1 and therefore endures nearly twice the failure load of L1. However, in both configurations, one would expect a similar linear-elastic deformation or a combined linear-elastic/plastic deformation. Instead, Fig. 15 reads as follows: Adding an extra UD-lamina changes the load–displacement curve from linear elastic to elastic–plastic. This conclusion appears misleading, and the authors of this paper remain inconclusive about the observations made in Fig. 15. Table 3. summarises the resulting mechanical properties.

4. Conclusion

The present study investigated the incorporation of tailored elastic behaviour in an inherently brittle epoxy-based fibre-reinforced composite material, achieved through a gradient interphase with a bio-based thermoplastic elastomer. The resulting multifunctional structure exhibits mechanical functionality, multi-scale toughening, and impact resistance within a shell structure. The epoxy system Araldite LY3585/Aradur 3475 was tested in combination with two different bio-based Pebax block copolymer grades, Pebax®Rnew®35R53 and Pebax®Rnew®1100. The interphase formation was characterised using optical hot-stage microscopy and Raman spectroscopy. Latter methods allowed for precise measurement of the spatial extent of the interphase region. Both Pebax grades exhibited an affinity towards the epoxy resin, whereby the diffusivity was significantly influenced by the polyamide 11 (PA11) content in the copolymer. Pebax®Rnew®35R53 with a PA11 content of 29 % displayed pronounced reaction–diffusion effects, including a reaction-induced phase-separated morphology, resulting in a brittle-to-ductile material gradient formed by a semi-interpenetrating network (s-IPN) Pebax®Rnew®35R53 achieved a maximum interphase thickness of 219 μm at 120 °C, while Pebax®Rnew®1100 achieved a maximum interphase thickness of 34 μm at 140 °C. This suggests that the optimal interphase thickness for Pebax®Rnew®35R53/epoxy is within the relevant curing cycles of the epoxy system. Subsequently, a composite laminate was manufactured from Pebax®Rnew®35R53/epoxy by combining fused filament fabrication with a vacuum infusion process, resulting in a structure with a flexible domain and variable stiffness properties. The laminate exhibited a brittle-to-ductile material architecture at the micrometre scale, demonstrating the combination of the two manufacturing processes and the structural concept. The resulting laminate showed a tailored, flexible response in the bending direction and stiff behaviour in the tensile direction. These findings provide valuable insights for designing and fabricating composite materials with desired mechanical functionality. Hence, the study successfully demonstrates the potential application of s-IPNs for integrating diverse functional regimes, such as multi-scale toughening, mechanical functionality, and impact resistance, in fibre-reinforced composite materials. This integration results in synergistic effects that enhance the overall performance of the generative material designs.

Funding

The authors acknowledge that this research was conducted utilizing internal resources, with additional financial support from a nationally-funded project [grant number 51573.1] by Innosuisse, Switzerland. We are grateful for the funding provided by Innosuisse, which has facilitated the successful execution of this research endeavour.

CRediT authorship contribution statement

Lucian Zweifel: Conceptualization, Methodology, Software, Investigation, Writing – original draft, Writing – review & editing, Visualization. **Julian Kupski:** Writing – original draft, Writing – review & editing. **Christian Brauner:** Conceptualization, Supervision, Project administration, Writing – original draft, Writing – review & editing.

Declaration of Competing Interest

The authors declare that they have no known competing financial interests or personal relationships that could have appeared to influence the work reported in this paper.

Data availability

Data will be made available on request.

Acknowledgements

The authors express their sincere gratitude to Huntsman Advanced Materials, represented by Klaus Ritter, for providing the necessary materials for this research project. Additionally, the support extended by Arkema is greatly appreciated.

References

[1] Ritchie RO. The conflicts between strength and toughness. Nat Mater 2011;10:817–22. https://doi.org/10.1038/nmat3115.
[2] Mimura K, Ito H, Fujioka H. Improvement of thermal and mechanical properties by control of morphologies in PES-modified epoxy resins. Polymer (Guildf) 2000;41:4451–9. https://doi.org/10.1016/S0032-3861(99)00700-4.
[3] Hodgkin JH, Simon GP, Varley RJ. Thermoplastic toughening of epoxy resins: a critical review. Polym Adv Technol 1998;9:3–10. https://doi.org/10.1002/(sici)1099-1581(199801)9:1<3::aid-pat727>3.3.co;2-9.
[4] Turmel DJ-P, Partridge IK. Heterogeneous phase separation around fibres in epoxy/PEI blends and its effect on composite delamination resistance. Compos Sci Technol 1997;57:1001–7. https://doi.org/https://doi.org/10.1016/S0266-3538(96)00148-0.
[5] Farooq U, Teuwen J, Dransfeld C. Toughening of Epoxy Systems with Interpenetrating Polymer Network (IPN): A Review. Polymers (Basel) 2020;12:1908. https://doi.org/https://doi.org/10.3390/polym12091908.
[6] Van Velthem P, Ballout W, Dumont D, Daoust D, Sclavons M, Cordenier F, et al. Phenoxy nanocomposite carriers for delivery of nanofillers in epoxy matrix for resin transfer molding (RTM)-manufactured composites. Compos Part A Appl Sci Manuf 2015;76:82–91. https://doi.org/10.1016/j.compositesa.2015.05.008.
[7] Grossman M, Pivovarov D, Bouville F, Dransfeld C, Masania K, Studart AR. Hierarchical Toughening of Nacre-Like Composites. Adv Funct Mater 2019;29:1806800. https://doi.org/10.1002/adfm.201806800.
[8] Rosetti Y, Alcouffe P, Pascault JP, Gérard JF, Lortie F. Polyether sulfone-based epoxy toughening: From micro- to nano-phase separation via PES end-chain modification and process engineering. Materials (Basel) 2018;11:1960. https://doi.org/10.3390/ma11101960.
[9] Lestriez B, Chapel JP, Gérard JF. Gradient interphase between reactive epoxy and glassy thermoplastic from dissolution process, reaction kinetics, and phase separation thermodynamics. Macromolecules 2001;34:1204–13. https://doi.org/10.1021/ma0012189.
[10] Miller-Chou BA, Koenig JL. A review of polymer dissolution. Prog Polym Sci 2003. https://doi.org/10.1016/S0079-6700(03)00045-5.
[11] S. LY, T. AT. Phase-Separated Interpenetrating Polymer Networks. Springer-Verlag Berlin Heidelberg; 2007. https://doi.org/10.1007/978-3-642-27154-0.
[12] Cugnoni J, Amacher R, Kohler S, Brunner J, Kramer E, Dransfeld C, et al. Towards aerospace grade thin-ply composites: Effect of ply thickness, fibre, matrix and interlayer toughening on strength and damage tolerance. Compos Sci Technol 2018;168:467–77. https://doi.org/10.1016/j.compscitech.2018.08.037.
[13] Teuwen JJE, Asquier J, Inderkum P, Masania K, Brauner C, Villegas IF, et al. Gradient interphases between high Tg epoxy and polyetherimide for advanced joining processes. Proc ECCM-18 Conf, Athens 2018.
[14] Zweifel L, Brauner C, Teuwen J, Dransfeld C. In Situ Characterization of the Reaction-Diffusion Behavior during the Gradient Interphase Formation of Polyetherimide with a High-Temperature Epoxy System. Polymers (Basel) 2022;14:435. https://doi.org/10.3390/polym14030435.
[15] Brauner C, Nakouzi S, Zweifel L, Tresch J. Co-curing behaviour of thermoset composites with a thermoplastic boundary layer for welding purposes. Adv Compos Lett 2020;29:1–9. https://doi.org/10.1177/2633366X20902777.
[16] Villegas IF, van Moorleghem R. Ultrasonic welding of carbon/epoxy and carbon/PEEK composites through a PEI thermoplastic coupling layer. Compos Part A Appl Sci Manuf 2018;109:75–83. https://doi.org/10.1016/j.compositesa.2018.02.022.
[17] Zweifel L, Ritter K, Brauner C. The Mechanical Characterization of Welded Hybrid Joints Based on a Fast-Curing Epoxy Composite with an Integrated Phenoxy Coupling Layer. Materials (Basel) 2022;15:1264. https://doi.org/10.3390/ma15031264.
[18] Zweifel L, Brauner C. Investigation of the interphase mechanisms and welding behaviour of fast-curing epoxy based composites with co-cured thermoplastic boundary layers. Compos Part A Appl Sci Manuf 2020;139:106120. https://doi.org/10.1016/j.compositesa.2020.106120.
[19] Aliyeva N, Sas HS, Saner OB. Recent developments on the overmolding process for the fabrication of thermoset and thermoplastic composites by the integration of nano/micron-scale reinforcements. Compos Part A Appl Sci Manuf 2021;149:106525. https://doi.org/10.1016/j.compositesa.2021.106525.
[20] Farooq U, Heuer S, Teuwen J, Dransfeld C. Effect of a Dwell Stage in the Cure Cycle on the Interphase Formation in a Poly(ether imide)/High Tg Epoxy System. ACS Appl Polym Mater 2021;3:6111–9. https://doi.org/10.1021/acsapm.1c00956.
[21] Olmos D, Bagdi K, Mózcó J, Pukánszky B, González-Benito J. Morphology and interphase formation in epoxy/PMMA/glass fiber composites: Effect of the molecular weight of the PMMA. J Colloid Interface Sci 2011;360:289–99. https://doi.org/10.1016/j.jcis.2011.04.028.
[22] Rastegar S, Mohammadi N, Bagheri R. Development of co-continuous morphology in epoxy poly(methyl methacrylate) (PMMA) blends cured by mixtures of phase-separating and non-phase-separating curing agents. Colloid Polym Sci 2004;283:145–53. https://doi.org/10.1007/s00396-004-1110-7.
[23] Olmos D, Arroyo JM, González-Benito J. Interphase morphology in glass fiber/PMMA modified epoxy matrix composites. Effect of molecular weight of PMMA. Polym Test 2012;31:785–91. https://doi.org/10.1016/j.polymertesting.2012.05.009.
[24] Ribeiro Salomão G, Gojzewski H, Erartsin O, Baran I. Novel co-bonded thermoplastic elastomer-epoxy/glass hybrid composites: The effect of cure temperature on the interphase morphology. Polym Test 2022;115:107736. https://doi.org/https://doi.org/10.1016/j.polymertesting.2022.107736.
[25] Erartsın O, Zanjani JSM, Baran I. Thermoset/Thermoplastic Interphases: The Role of Initiator Concentration in Polymer Interdiffusion. Polymers (Basel) 2022;14:1493. https://doi.org/10.3390/polym14071493.
[26] Bodkhe S, Ermanni P. 3D printing of multifunctional materials for sensing and actuation: Merging piezoelectricity with shape memory. Eur Polym J 2020;132:109738. https://doi.org/10.1016/j.eurpolymj.2020.109738.
[27] Lendlein A, Trask RS. Multifunctional materials: Concepts, function-structure relationships, knowledge-based design, translational materials research. Multifunct Mater 2018;1. https://doi.org/10.1088/2399-7532/aada7b.
[28] Hajiesmaili E, Clarke DR. Reconfigurable shape-morphing dielectric elastomers using spatially varying electric fields. Nat Commun 2019;10:183. https://doi.org/10.1038/s41467-018-08094-w.
[29] Fasel U, Keidel D, Baumann L, Cavolina G, Eichenhofer M, Ermanni P. Composite additive manufacturing of morphing aerospace structures. Manuf Lett 2020;23:85–8. https://doi.org/10.1016/j.mfglet.2019.12.004.
[30] Ahmadi A, Asgari M. Novel bio-inspired variable stiffness soft actuator via fiber-reinforced dielectric elastomer, inspired by Octopus bimaculoides. Intell Serv Robot 2021;14:691–705. https://doi.org/10.1007/s11370-021-00388-1.
[31] Shintake J, Rosset S, Schubert BE, Floreano D, Shea HR. A Foldable Antagonistic Actuator. IEEE/ASME Trans. Mechatronics 2015;20. https://doi.org/10.1109/TMECH.2014.2359337.
[32] Imamura H, Kadooka K, Taya M. A variable stiffness dielectric elastomer actuator based on electrostatic chucking. Soft Matter 2017;13. https://doi.org/10.1039/c7sm00546f.
[33] Zhou L, Ren L, Chen Y, Niu S, Han Z, Ren L. Bio-Inspired Soft Grippers Based on Impactive Gripping. Adv Sci 2021;8:2002017. https://doi.org/10.1002/advs.202002017.
[34] Yang W, Chen IH, Gludovatz B, Zimmermann EA, Ritchie RO, Meyers MA. Natural flexible dermal armor. Adv Mater 2013;25:31–48. https://doi.org/10.1002/adma.201202713.
[35] Zimmermann EA, Gludovatz B, Schaible E, Dave NKN, Yang W, Meyers MA, et al. Mechanical adaptability of the Bouligand-type structure in natural dermal armour. Nat Commun 2013;4:2634. https://doi.org/10.1038/ncomms3634.
[36] Lligadas G, Ronda JC, Galià M, Cádiz V. Renewable polymeric materials from vegetable oils: A perspective. Mater Today 2013;16:337–43. https://doi.org/10.1016/j.mattod.2013.08.016.
[37] Glass Fibre Fabric n.d. https://shop.swiss-composite.ch/pi.php/Verstaerkungsfasern/Glasfasern/Glasgewebe/Glasgewebe-Silan-163gm2-Koeper-160cm.html (accessed 2 December 2022).
[38] Schär M, Zweifel L, Arslan D, Grieder S, Maurer C, Brauner C. Fused Filament Fabrication of Bio-Based Polyether-Block-Amide Polymers (PEBAX) and Their Related Properties. Polymers (Basel) 2022;14:5092. https://doi.org/10.3390/polym14235092.
[39] Arslan D. 3D printing of Phenoxy - Filament production, process parameters and application potential. Hamburg: Sampe Conf; 2022.
[40] Palardy G, Villegas IF. Smart ultrasonic welding of thermoplastic composites. Proc Am Soc Compos - 31st Tech Conf ASC 2016, 2016..

[41] Hein R. Vorhersage und In-Situ Bewertung fertigungsbedingter Deformationen und Eigenspannungen von Kompositen. Braunschweig: Deutsches Zentrum für Luft- und Raumfahrt e.V; 2019.
[42] Datasheet Pebax® Rnew® 35R53 SP 01 n.d. https://www.materialdatacenter.com/ms/en/Pebax/Arkema/Pebax®+Rnew®+35R53+SP+01/2e6a1621/264 (accessed 28 September 2022).
[43] Datasheet PEBAX® RNEW® 1100 n.d. https://www.arkema.com/global/en/products/product-finder/product-range/technicalpolymers/pebax-product-family/ (accessed 27 October 2022).